Effect of simple shear on liquid drainage within foams

S. J. Neethling
Department of Earth Science and Engineering, Imperial College, London SW7 2AZ, United Kingdom
(Received 16 September 2005; revised manuscript received 27 February 2006; published 29 June 2006)

This paper examines the impact of shear on the drainage of liquid through a foam. The effect on drainage of changes in the Plateau border network brought about by shear is examined. This effect of shear was modeled using both a detailed three-dimensional simulation of foam structure, and an idealized two-dimensional hexagonal foam. The main phenomenon that has been discovered is that shear induces an anisotropy in the drainage of liquid through the foam. If the foam is strained and liquid flows under gravity either perpendicular or parallel to the shear direction, a net liquid flow in the direction perpendicular to the direction of gravity is induced. It was found that the degree of anisotropy increases nearly linearly with increasing strain until the foam yields, after which the degree of flow anisotropy remains roughly constant. This is not a small effect, with the flow in the direction perpendicular to gravity being up to about 20% of the flow in the direction of gravity at the yield strain. This shear-induced anisotropy provides a potential explanation for the hitherto puzzling phenomenon of the convective roll in foam. The other two effects examined are the effect of shear on the length of Plateau borders per volume of foam, which increases as strain increases, and the resistance of the foam to flow in the direction of gravity, which increases if the strain direction is perpendicular to gravity, but decreases if the strain is parallel to gravity.

DOI: 10.1103/PhysRevE.73.061408 PACS number(s): 82.70.Rr, 83.80.Iz

I. INTRODUCTION

There have been both experimental [1] and theoretical [2–4] studies of the rheological properties of foams, especially their elastic response to small applied strains. In particular, these studies have considered the impact of the foam liquid fraction on the shear behavior. In turn, studies on the effect of shear on the foam drainage [5,6] have focused on shear dilatancy. In contrast, this paper will concentrate on the effect of shear on foam drainage as a result of changes in the foam structure.

This study simulates the liquid flow through individual Plateau borders in foam. Unsheared foam results are similar to those predicted by the continuum drainage equation [7,8]; however, as the foam is sheared and the structure changes, the drainage behavior deviates from that predicted by existing drainage theory. One of the major impacts of shear on liquid drainage that will be demonstrated in this paper is that the structural anisotropy generated by the shear results in a drainage anisotropy. It will be shown that in a sheared foam there is a substantial net liquid flow component in a direction perpendicular to the gravitational driving force.

II. SIMULATION METHOD

All the three-dimensional (3D) foams simulated in this work are random and monodispersed. The foams are also assumed to have low liquid content. This means that the structure can be simulated with the Plateau borders assumed to be lines with no volume or surface area. The Plateau borders are also assumed to be small enough that gravitational forces are negligible compared to surface forces. These assumptions mean that the simulation of the structural changes brought about by shear and the drainage can be carried out in sequential steps, which greatly simplifies the calculations.

The three-dimensional simulations presented in this work are the result of the simulation procedure that is outlined below.

A. Generating the initial structure

A periodic random Voronoi tessellation was used as a starting topology. Spatial placement restrictions on the points used to generate the tessellation resulted in a practically monodispersed volume distribution (Fig. 1). In the subsequent surface minimization, the bubble volumes are adjusted so as to produce a monodispersed foam structure.

A minimum surface area structure based on the topology generated in the Voronoi tessellation was obtained using SURFACE EVOLVER [9]. This is equivalent to a low liquid content foam at equilibrium, since these systems are dominated by surface forces. Topological rearrangements were carried out

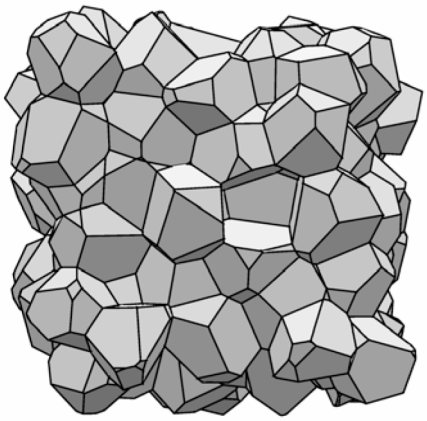

FIG. 1. An example of a periodic three-dimensional Voronoi tessellation used as a starting structure. This is not a minimum surface area structure, but it is topologically similar to a foam.

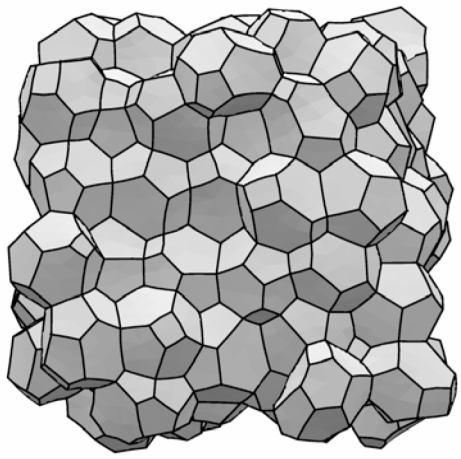

FIG. 2. The monodispersed random and periodic foam structure produced using the Voronoi tessellation in Fig. 1. This is a minimum surface area structure and is thus both topologically and geometrically representative of a foam structure.

as film areas or Plateau border lengths became small.

In order to eliminate some of the trapped stresses and reduce the structure to a lower-energy state, an annealing procedure was used in which small compressional strains are applied to each principal axis in turn (this procedure is similar to that used by Kraynik *et al.* [10]). Figure 2 shows a typical foam structure obtained after the annealing process.

The simulated foam structures are fully periodic to avoid edge effects and to allow relatively small numbers of bubbles, either 125 or 216 in a periodic cell, to be used. These simulated foam structures are the starting structure for the shear simulations.

B. Shear simulations

Simple shear was simulated by distorting the periodic cell in the x direction on the x-y plane. The shear is characterized in terms of the strain γ, the amount of deflection in the x direction per distance in the y direction. Predictions for drainage in different directions are achieved by changing the direction of gravity.

The foam structure is assumed to be quasistatic, and for each applied strain the surface area was minimized before the liquid flow through the structure was calculated. Figure 3 gives an example of a sequence of sheared foam structures. Note that the strain was increased in increments of 0.02 and so the structures shown in Fig. 3 do not represent a comprehensive sequence.

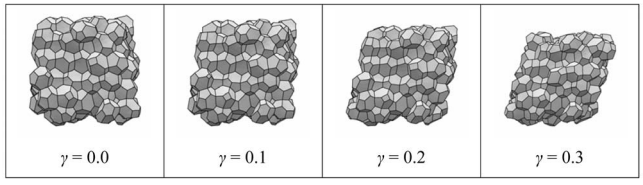

FIG. 3. Evolution of the foam structure as strain is increased.

C. Drainage calculations

The aim of this paper is to calculate the impact of shear-induced changes in foam structure on the liquid drainage through the foam. The drainage calculations will only consider drainage along the Plateau borders, as they contain most of the liquid in reasonably dry foams [11].

SURFACE EVOLVER discretizes the foam structure and therefore the extracted Plateau border network consists of interconnected segments. An individual Plateau border consists of many of these straight segments, allowing the curvature of the Plateau borders to be approximated.

In each Plateau border segment the gravity, capillary suction, and viscous drag forces [7,8] balance. A force balance yields an equation describing the volumetric flow rate in a Plateau border, Q_{PB}, with a single dependent variable A, the cross-sectional area of the Plateau border [Eq. (1)]. The flow rate Q_{PB} is a function of the distance along the Plateau border, l, the component of gravity along the Plateau border, g^*, the liquid density ρ, the surface tension σ, and the viscosity μ. C_{PB} is the Plateau border drag coefficient, which has a value of approximately 50 for immobile interfaces [7] and a lower value as the interfacial mobility increases:

$$Q_{PB} = k_1 A^2 - k_2 \sqrt{A} \frac{dA}{dl},$$

$$k_1 = \frac{\rho g^*}{C_{PB}\mu},$$

$$k_2 = \frac{\sigma\sqrt{\sqrt{3} - \pi/2}}{2C_{PB}\mu}. \tag{1}$$

The constant in k_2 is a shape factor based on the cross-sectional area of the Plateau border.

The periodic nature of the simulations means that the liquid content does not vary at the scale of the unit cell. This means that the liquid content in these simulations is macroscopically uniform. There is therefore no macroscopic capillary-driven flow. If individual Plateau borders curve, though, there can be local variations in the liquid content. This is because a curving Plateau border will have a changing gravitational component along the Plateau border (i.e., k_1 will be a function of l). At steady state an individual Plateau border must have the same liquid flow at all points along its length and so the value of A changes as it curves.

If all the Plateau borders in a system with macroscopically uniform liquid content were straight and they met at the tetrahedral angle at the vertices, then there would be no local variations in A. This is an impossible condition to meet in a 3D foam. Typically, though, most of the internal Plateau borders in a foam have very little curvature (Figs. 2 and 3). It will therefore be assumed that the local variations in the cross-sectional Plateau border area are small and do not have a major impact on the drainage behavior of the foam. (See Appendix A for a comparison between a detailed simulation in which the local liquid content variations are accounted for and the simplified calculations used in this work.) Note that by dividing the Plateau borders up into segments, the curva-

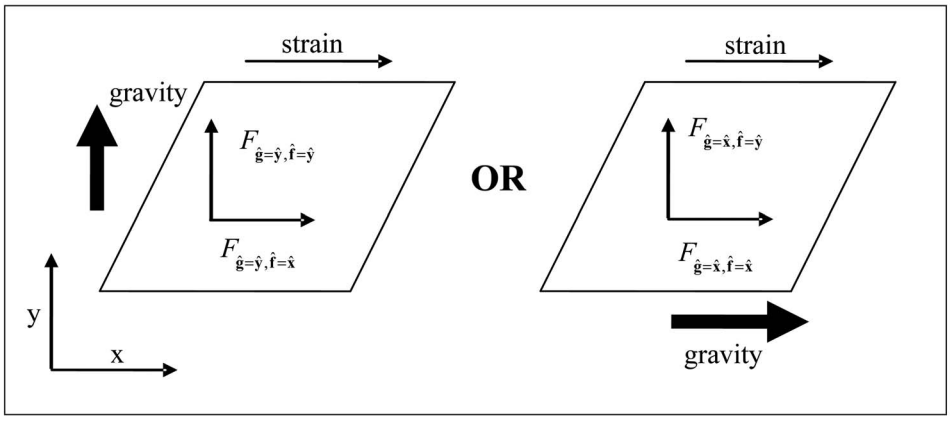

FIG. 4. The two drainage cases being studied and the notation used to indicate the direction of gravity and flux being considered. Note that the first subscript to the flux indicates the direction of gravity and the second the direction of the flux being considered.

ture of the Plateau borders is still included in the calculations. It is only the variations in cross-sectional Plateau border area brought about by these curvatures that are ignored. This means that Eq. (1) takes the following approximate form if $\hat{\mathbf{g}}$ is a unit vector in the direction of gravity and $\boldsymbol{l}_i$ is a vector along the Plateau border segment i ($|\boldsymbol{l}_i|$ is the length of the segment):

$$Q_{PB,i} \approx \frac{\rho g \dfrac{\boldsymbol{l}_i \cdot \hat{\mathbf{g}}}{|\boldsymbol{l}_i|}}{C_{PB}\mu} A^2, \tag{2}$$

where $Q_{PB,i}$ is the volumetric flow rate in Plateau border segment i and g is the gravitational acceleration.

Since the calculation of flow anisotropies is one of the objectives of this paper, it is desirable that the average net flux in directions not necessarily the same as gravity should be calculated. For this purpose a unit vector $\hat{\mathbf{f}}$ in the direction of flow being considered is defined.

In order to calculate the net flux in direction $\hat{\mathbf{f}}$ we need to calculate the flux through a plane perpendicular to $\hat{\mathbf{f}}$. This means that a Plateau border segment will contribute to the flux only if it intersects the plane.

It is possible to improve the accuracy of the estimated flux by integrating over all planes perpendicular to $\hat{\mathbf{f}}$. Since the integration over all planes proceeds in the direction $\hat{\mathbf{f}}$, the contribution of an individual Plateau border segment to this averaged flux will be proportional to the component of the segment length in the direction $\hat{\mathbf{f}}$ (i.e., $\boldsymbol{l}_i \cdot \hat{\mathbf{f}}$). The integration over a segment is simply the product of this projected length and the flow rate, since this flow is constant along the length of a segment. By summing the contributions of all the Plateau border segments, the following equation for the average flux in direction $\hat{\mathbf{f}}$ is obtained:

$$F_{\hat{\mathbf{g}},\hat{\mathbf{f}}} = \frac{\sum Q_{PB,i} \boldsymbol{l}_i \cdot \hat{\mathbf{f}}}{V}, \tag{3}$$

where V is the volume of the region of interest, which appears as a result of the multiplication of the area over which the flux is calculated (i.e., the area of the plane) multiplied by the distance over which the planes contributing to the flux are integrated.

By substituting Eq. (2) into Eq. (3), the following expression for the average flux in the $\hat{\mathbf{f}}$ direction for gravity in the $\hat{\mathbf{g}}$ direction is obtained:

$$F_{\hat{\mathbf{g}},\hat{\mathbf{f}}} \approx \frac{\rho g A^2}{C_{PB}\mu V} \sum \left(\frac{\boldsymbol{l}_i \cdot \hat{\mathbf{g}}}{|\boldsymbol{l}_i|} \boldsymbol{l}_i \cdot \hat{\mathbf{f}} \right). \tag{4}$$

While Eq. (4) can be used to calculate the average flux in any direction with gravity in any direction, two particular directions are examined in detail in this paper, namely, parallel and perpendicular to the shear direction. Since the shear is in the x direction, this requires a unit vector in the x direction, $\hat{\mathbf{x}}$, and one in the y direction, $\hat{\mathbf{y}}$. The strain direction and the various combinations of gravitational and flux components being considered in this work are illustrated in Fig. 4.

If Δx_i, Δy_i, and Δz_i are the components of the Plateau border segment i in the x, y, and z directions, respectively, then

$$\Delta x_i = \boldsymbol{l}_i \cdot \hat{\mathbf{x}}, \quad \Delta y_i = \boldsymbol{l}_i \cdot \hat{\mathbf{y}}, \quad \Delta z_i = \boldsymbol{l}_i \cdot \hat{\mathbf{z}}. \tag{5}$$

Equations (4) and (5) can be combined in order to give formulas for the four combinations of gravitational and flux component directions illustrated in Fig. 4 (note that shear is always in the x direction):

$$F_{\hat{\mathbf{g}}=\hat{\mathbf{y}},\hat{\mathbf{f}}=\hat{\mathbf{y}}} \approx K \sum \frac{(\boldsymbol{l}_i \cdot \hat{\mathbf{y}})^2}{|\boldsymbol{l}_i|} = K \sum \frac{\Delta y_i^2}{\sqrt{\Delta x_i^2 + \Delta y_i^2 + \Delta z_i^2}}, \tag{6}$$

$$F_{\hat{\mathbf{g}}=\hat{\mathbf{x}},\hat{\mathbf{f}}=\hat{\mathbf{y}}} \approx F_{\hat{\mathbf{g}}=\hat{\mathbf{y}},\hat{\mathbf{f}}=\hat{\mathbf{x}}} \approx K \sum \frac{(\boldsymbol{l}_i \cdot \hat{\mathbf{x}})(\boldsymbol{l}_i \cdot \hat{\mathbf{y}})}{|\boldsymbol{l}_i|} = K \sum \frac{\Delta y_i \Delta x_i}{\sqrt{\Delta x_i^2 + \Delta y_i^2 + \Delta z_i^2}}, \tag{7}$$

$$F_{\hat{\mathbf{g}}=\hat{\mathbf{x}},\hat{\mathbf{f}}=\hat{\mathbf{x}}} \approx K \sum \frac{(\boldsymbol{l}_i \cdot \hat{\mathbf{x}})^2}{|\boldsymbol{l}_i|} = K \sum \frac{\Delta x_i^2}{\sqrt{\Delta x_i^2 + \Delta y_i^2 + \Delta z_i^2}}, \tag{8}$$

where $K = (\rho g / V C_{PB} \mu) A^2$.

Note that Δx_i, Δy_i, and Δz_i have signs, though it is immaterial which end of an individual Plateau border segment is considered to be the beginning or the end. A potential con-

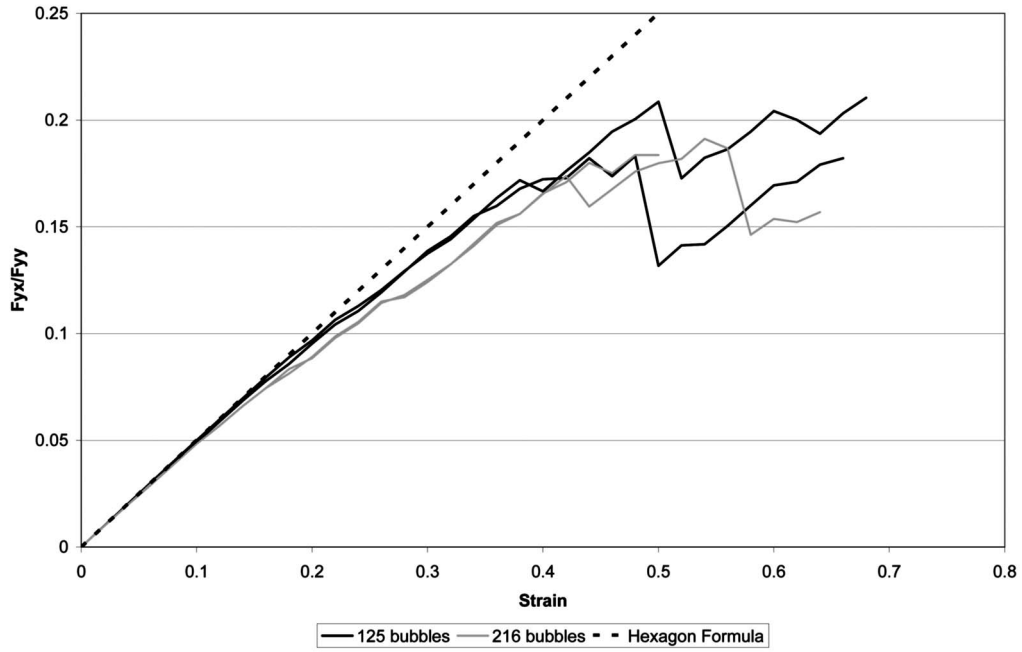

FIG. 5. Relative flow anisotropy for gravity in the y direction (shear in the x direction) as a function of strain. Legend indicates number of bubbles in the periodic cell.

cern with this equation is that the calculated flux will change if the structure is refined. The calculated flux does not change with refinement (see Appendix B), unless the surface area of the structure is further minimized after refinement, in which case there will be subtle changes in the calculated flux.

The most relevant of these formulas for the purposes of this paper is Eq. (7), since it gives the value of the anisotropic flux (that is, the flux in the direction perpendicular to the applied gravitational driving force). In an isotropic foam structure, this flux would be expected to be zero. It can be seen from Eq. (7) that $F_{\hat{\mathbf{g}}=\hat{\mathbf{x}},\hat{\mathbf{k}}=\hat{\mathbf{y}}}=F_{\hat{\mathbf{g}}=\hat{\mathbf{y}},\hat{\mathbf{k}}=\hat{\mathbf{x}}}$ not only for an isotropic unsheared foam, but also for any sheared foam as well. In fact, for any perpendicular pair of directions, the magnitude of the anisotropic flux will be the same whether gravity is in one direction and the flux measured in the other direction, or vice versa.

In order to aid analysis a dimensionless relative flow anisotropy is introduced. This is the ratio of the flux in the direction perpendicular to gravity to that parallel to gravity.

The relative anisotropy for gravity in the y direction (gravity perpendicular to the shear direction) is

$$\frac{F_{\hat{\mathbf{g}}=\hat{\mathbf{y}},\hat{\mathbf{f}}=\hat{\mathbf{x}}}}{F_{\hat{\mathbf{g}}=\hat{\mathbf{y}},\hat{\mathbf{f}}=\hat{\mathbf{y}}}} \approx \frac{\sum \frac{(\boldsymbol{l}_i\cdot\hat{\mathbf{x}})(\boldsymbol{l}_i\cdot\hat{\mathbf{y}})}{|\boldsymbol{l}_i|}}{\sum \frac{(\boldsymbol{l}_i\cdot\hat{\mathbf{y}})^2}{|\boldsymbol{l}_i|}} = \frac{\sum \frac{\Delta y_i \Delta x_i}{\sqrt{\Delta x_i^2+\Delta y_i^2+\Delta z_i^2}}}{\sum \frac{\Delta y_i^2}{\sqrt{\Delta x_i^2+\Delta y_i^2+\Delta z_i^2}}}. \tag{9}$$

The relative anisotropy for gravity in the x direction (gravity parallel to the shear direction) is

$$\frac{F_{\hat{\mathbf{g}}=\hat{\mathbf{x}},\hat{\mathbf{f}}=\hat{\mathbf{y}}}}{F_{\hat{\mathbf{g}}=\hat{\mathbf{x}},\hat{\mathbf{f}}=\hat{\mathbf{x}}}} \approx \frac{\sum \frac{(\boldsymbol{l}_i\cdot\hat{\mathbf{x}})(\boldsymbol{l}_i\cdot\hat{\mathbf{y}})}{|\boldsymbol{l}_i|}}{\sum \frac{(\boldsymbol{l}_i\cdot\hat{\mathbf{x}})^2}{|\boldsymbol{l}_i|}} = \frac{\sum \frac{\Delta y_i \Delta x_i}{\sqrt{\Delta x_i^2+\Delta y_i^2+\Delta z_i^2}}}{\sum \frac{\Delta x_i^2}{\sqrt{\Delta x_i^2+\Delta y_i^2+\Delta z_i^2}}}. \tag{10}$$

Note that these relative flow anisotropies depend only on the structure of the foam, since all the parameters relating to the fluid properties cancel.

III. SHEAR-INDUCED FLOW ANISOTROPIES

A. Shearing a three-dimensional foam

In order to ascertain how the drainage responds to the shear, Eqs. (9) and (10) have been applied to the Plateau border networks extracted from a series of SURFACE EVOLVER–based strain simulations (Sec. II B). In Figs. 5 and 6 the ratio of the net flux perpendicular to gravity to that parallel to gravity (the relative flow anisotropy) in a three-dimensional foam is plotted as a function of the applied macroscopic strain. For comparison, the solution for a sheared two-dimensional hexagonal foam (hexagonal formula) is also given (see Sec. III B).

The drainage behavior is similar whether gravity is perpendicular to the shear (Fig. 5), or in the same direction as the shear (Fig. 6). In both cases there is an initial increase in the relative anisotropy up to a strain of about 0.4–0.5 after which the ratio remains reasonably constant, albeit with some fluctuations (the fluctuations are due to the finite size of the simulated samples). The point at which this transition occurs corresponds to the yield strain of the foam.

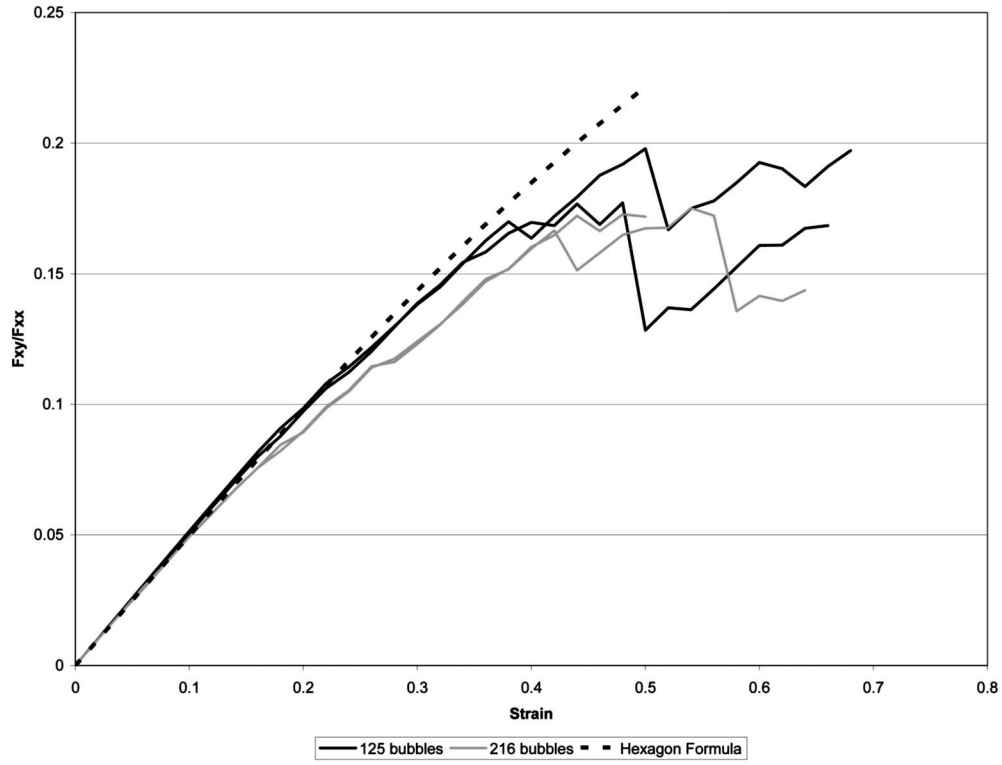

FIG. 6. Relative flow anisotropy for gravity in the x direction (shear in the x direction) as a function of strain. Legend indicates number of bubbles in the periodic cell.

The difference between these curves is not due to differences in the magnitudes of the anisotropic fluxes, which are identical [Eq. (7)], but is rather because the shear also has an impact on the flow parallel to gravity (see Sec. IV B).

It should be noted that this flow anisotropy is potentially quite a large effect. At the yield strain, the net flux in the direction perpendicular to gravity is of the order of 15–20 % of the flux parallel to gravity.

The flow anisotropy in the direction perpendicular to the shear plane (the z direction) is not shown since, as expected, shear has no real impact on this flow. The flow in the z direction for gravity in either the x or y direction is never more than 1% of the gravity-driven flow and there is no systematic change with strain, only slight fluctuations brought about by topological changes within the structure. The only reason the z direction anisotropy is not exactly zero is because the initial structures are finite in size and not perfectly isotropic. There cannot be a preferential direction for shear-induced flow perpendicular to shear plane since mirroring the structure in this direction does not change the sign of the strain, while mirroring the structure in either of the other directions does change the sign of the strain.

B. Shearing a hexagonal foam

A hexagonal two-dimensional foam allows simple relationships for the degree of anisotropy to be derived, which can be compared to the results from the full three-dimensional simulations.

In a regular hexagonal foam, drainage calculations can be performed using a unit cell of half of three films (Fig. 7). Only half the parallelogram connecting the centers of four hexagons need be considered, since the identical films are repeated in each half of the parallelogram, albeit in a different order [Eqs. (6)–(10) are not dependent on the actual layout of the films, only the components of the lengths in each direction].

The vertex where the edges meet is the Steiner point of the triangle. The Steiner point coordinate is a function of the macroscopic strain γ and the triangle width l [12]. If the origin for these coordinates is the midpoint of the triangle base, then the Steiner point is

$$x_S = \frac{l\gamma}{\sqrt{3}\left[\left(\frac{\gamma}{2}\right)^2 + 1\right]},$$

$$y_S = \frac{2l}{\sqrt{3}\left[\left(\frac{\gamma}{2}\right)^2 + 1\right]} - \frac{\sqrt{3}}{2}l, \tag{11}$$

The lengths of the x and y components of the three relevant edge segments are as follows:

$$\Delta x_1 = \frac{l}{2} + x_S, \quad \Delta y_1 = y_s$$

$$\Delta x_2 = \frac{l}{2} - x_S, \quad \Delta y_2 = -y_s$$

$$\Delta x_3 = \frac{\sqrt{3}}{2} l\gamma - x_S, \quad \Delta y_3 = \frac{\sqrt{3}}{2} l - y_s. \tag{12}$$

In order to use these equations to calculate fluxes, the valid ranges for the relevant variables need to be defined. First, the triangle side length must be positive ($l>0$). Second, the strain must be less than the strain at which a topological change will occur. This happens when one of the edge lengths becomes zero. As the strain increases, the edge that shrinks is edge 2. This edge disappears when $y_s=0$, which means that the valid range for strain is

$$|\gamma| < \frac{2}{\sqrt{3}}. \tag{13}$$

Using Eqs. (6)–(8), together with Eqs. (11) and (12) above and noting the valid ranges for the variables, the following relationships are obtained:

$$F_{\hat{\mathbf{g}}=\hat{\mathbf{y}},\hat{\mathbf{f}}=\hat{\mathbf{y}}} = K \frac{\sqrt{3} l}{2\sqrt{\left(\frac{\gamma}{2}\right)^2 + 1}}, \tag{14}$$

$$F_{\hat{\mathbf{g}}=\hat{\mathbf{x}},\hat{\mathbf{f}}=\hat{\mathbf{y}}} = F_{\hat{\mathbf{g}}=\hat{\mathbf{y}},\hat{\mathbf{f}}=\hat{\mathbf{x}}} = K \frac{\sqrt{3} l\gamma}{4\sqrt{\left(\frac{\gamma}{2}\right)^2 + 1}}, \tag{15}$$

$$F_{\hat{\mathbf{g}}=\hat{\mathbf{x}},\hat{\mathbf{f}}=\hat{\mathbf{x}}} = K \frac{\sqrt{3} l(\gamma^2 + 2)}{4\sqrt{\left(\frac{\gamma}{2}\right)^2 + 1}}. \tag{16}$$

When the above equations are combined to give the relative flow anisotropies in a 2D hexagonal foam, quite simple expressions are obtained. The relative anisotropy for gravity in the y direction is given by

$$\frac{F_{\hat{\mathbf{g}}=\hat{\mathbf{y}},\hat{\mathbf{f}}=\hat{\mathbf{x}}}}{F_{\hat{\mathbf{g}}=\hat{\mathbf{y}},\hat{\mathbf{f}}=\hat{\mathbf{y}}}} = \frac{\gamma}{2}, \tag{17}$$

and the relative anisotropy for gravity in the x direction is

$$\frac{F_{\hat{\mathbf{g}}=\hat{\mathbf{x}},\hat{\mathbf{f}}=\hat{\mathbf{y}}}}{F_{\hat{\mathbf{g}}=\hat{\mathbf{x}},\hat{\mathbf{f}}=\hat{\mathbf{x}}}} = \frac{\gamma}{2\left[\left(\frac{\gamma}{2}\right)^2 + 1\right]}. \tag{18}$$

The above equations show that in a hexagonal foam the relative flow anisotropy increases linearly if the strain is perpendicular to gravity. For gravity parallel to the strain direction, the relationship is nearly linear at low strains, but progressively deviates from linearity as the strain increases.

From Figs. 5 and 6 it can be seen that below the yield strain the relative flow anisotropy for the three-dimensional foam is predicted quite well by the hexagonal formulas. This is to be expected, since even in a three-dimensional foam, the shearing is an essentially two-dimensional effect, since it does not result in much movement of the Plateau borders in the direction perpendicular to the shear plane (the z direction in these simulations).

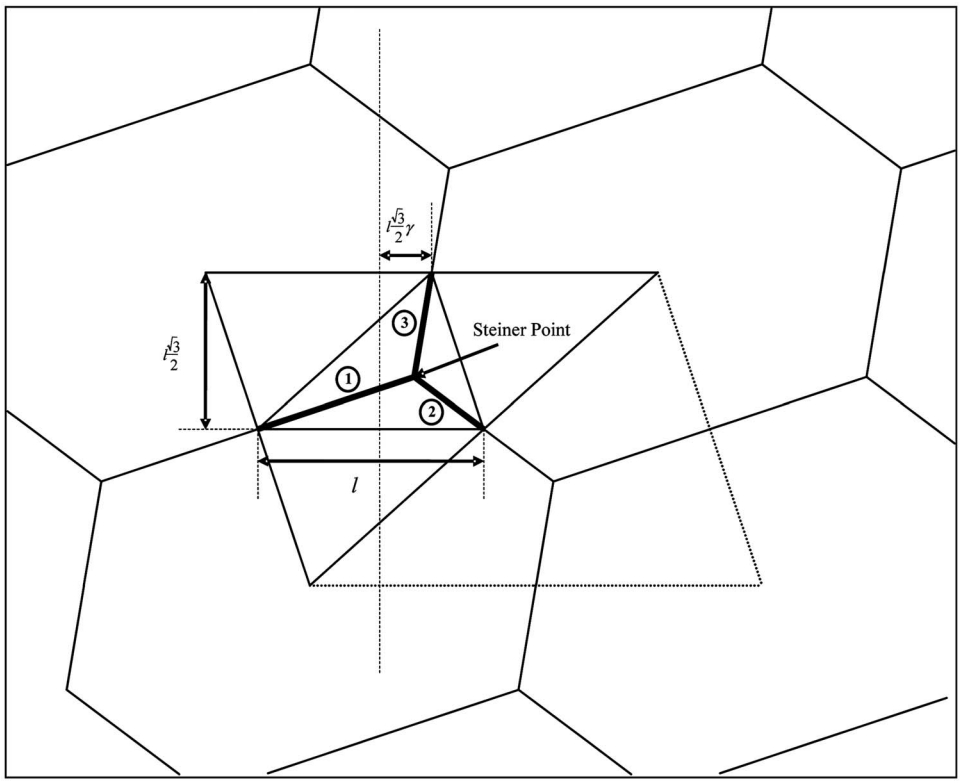

FIG. 7. A sheared hexagonal foam showing the periodic cell used for calculations. The numbers in the circles refer to the edge numbers in Eq. (12).

While Eqs. (17) and (18) provide quite good approximations for the behavior of the three-dimensional foam below the yield strain, there is a progressive overprediction of the relative flow anisotropy as the strain increases (Figs. 5 and 6). Since the three-dimensional foams are disordered, topological changes can occur at strains much lower than the yield strain. These topological changes release stress and thus allow the apparent local strain to be less than the applied macroscopic strain experienced by the foam. The relative anisotropy is therefore reduced to below what might be expected in the absence of topological changes.

C. Flow at other angles

Thus far this paper has concentrated on the effect of shear on drainage in which the direction of gravity is either parallel or perpendicular to the shear direction. It has been shown that the effect of shear on the degree of flow anisotropy was largely the same whether the flow was parallel or perpendicular to the shear direction.

In this section, the effect of shear will be examined for gravity at other angles. Gravity will be set at an angle of θ, from the vertical (unit vector $\hat{\mathbf{r}}$), while two flow directions will be considered, one parallel to gravity (unit vector $\hat{\mathbf{r}}$) and one perpendicular to gravity (unit vector $\hat{\mathbf{r}}_\perp$, 90° clockwise from $\hat{\mathbf{r}}$). The net fluxes in the two relevant flow directions can be written as follows [from Eq. (4)]. For flow parallel to gravity,

$$F_{\hat{\mathbf{g}}=\hat{\mathbf{r}},\hat{\mathbf{f}}=\hat{\mathbf{r}}} \approx \frac{\rho g A^2}{C_{PB}\mu V}\sum\left(\frac{(\boldsymbol{l}_i\cdot\hat{\mathbf{r}})^2}{|\boldsymbol{l}_i|}\right), \tag{19}$$

and for flow perpendicular to gravity,

$$F_{\hat{\mathbf{g}}=\hat{\mathbf{r}},\hat{\mathbf{f}}=\hat{\mathbf{r}}_\perp} \approx \frac{\rho g A^2}{C_{PB}\mu V}\sum\left(\frac{\boldsymbol{l}_i\cdot\hat{\mathbf{r}}}{|\boldsymbol{l}_i|}\boldsymbol{l}_i\cdot\hat{\mathbf{r}}_\perp\right). \tag{20}$$

This can be expanded and written according to already investigated relationships by noting that $\hat{\mathbf{r}}=\hat{\mathbf{x}}\sin\theta+\hat{\mathbf{y}}\cos\theta$ and $\hat{\mathbf{r}}_\perp=\hat{\mathbf{x}}\cos\theta-\hat{\mathbf{y}}\sin\theta$:

$$\begin{aligned}F_{\hat{\mathbf{g}}=\hat{\mathbf{r}},\hat{\mathbf{f}}=\hat{\mathbf{r}}} &= \frac{\rho g A^2}{C_{PB}\mu V}\sum\left(\sin^2\theta\frac{(\boldsymbol{l}_i\cdot\hat{\mathbf{x}})^2}{|\boldsymbol{l}_i|}\right.\\ &\quad\left.+2\sin\theta\cos\theta\frac{(\boldsymbol{l}_i\cdot\hat{\mathbf{x}})(\boldsymbol{l}_i\cdot\hat{\mathbf{y}})}{|\boldsymbol{l}_i|}+\cos^2\theta\frac{(\boldsymbol{l}_i\cdot\hat{\mathbf{y}})^2}{|\boldsymbol{l}_i|}\right)\\ &= \sin^2\theta F_{\hat{\mathbf{g}}=\hat{\mathbf{x}},\hat{\mathbf{f}}=\hat{\mathbf{x}}}+2\sin\theta\cos\theta F_{\hat{\mathbf{g}}=\hat{\mathbf{x}},\hat{\mathbf{f}}=\hat{\mathbf{y}}}\\ &\quad+\cos^2\theta F_{\hat{\mathbf{g}}=\hat{\mathbf{y}},\hat{\mathbf{f}}=\hat{\mathbf{y}}},\end{aligned} \tag{21}$$

$$\begin{aligned}F_{\hat{\mathbf{g}}=\hat{\mathbf{r}},\hat{\mathbf{f}}=\hat{\mathbf{r}}_\perp} &= \frac{\rho g A^2}{C_{PB}\mu V}\sum\left(\sin\theta\cos\theta\frac{(\boldsymbol{l}_i\cdot\hat{\mathbf{x}})^2}{|\boldsymbol{l}_i|}+(2\cos^2\theta\right.\\ &\quad\left.-1)\frac{(\boldsymbol{l}_i\cdot\hat{\mathbf{x}})(\boldsymbol{l}_i\cdot\hat{\mathbf{y}})}{|\boldsymbol{l}_i|}-\sin\theta\cos\theta\frac{(\boldsymbol{l}_i\cdot\hat{\mathbf{y}})^2}{|\boldsymbol{l}_i|}\right)\\ &= \sin\theta\cos\theta F_{\hat{\mathbf{g}}=\hat{\mathbf{x}},\hat{\mathbf{f}}=\hat{\mathbf{x}}}+(2\cos^2\theta-1)F_{\hat{\mathbf{g}}=\hat{\mathbf{x}},\hat{\mathbf{f}}=\hat{\mathbf{y}}}\\ &\quad-\sin\theta\cos\theta F_{\hat{\mathbf{g}}=\hat{\mathbf{y}},\hat{\mathbf{f}}=\hat{\mathbf{y}}}.\end{aligned} \tag{22}$$

The relative anisotropy can be calculated using Eqs. (21) and (22):

$$\frac{F_{\hat{\mathbf{g}}=\hat{\mathbf{r}},\hat{\mathbf{f}}=\hat{\mathbf{r}}_\perp}}{F_{\hat{\mathbf{g}}=\hat{\mathbf{r}},\hat{\mathbf{f}}=\hat{\mathbf{r}}}} = \frac{\tan\theta\left(\frac{F_{\hat{\mathbf{g}}=\hat{\mathbf{x}},\hat{\mathbf{f}}=\hat{\mathbf{x}}}}{F_{\hat{\mathbf{g}}=\hat{\mathbf{y}},\hat{\mathbf{f}}=\hat{\mathbf{y}}}}-1\right)+(1-\tan^2\theta)\frac{F_{\hat{\mathbf{g}}=\hat{\mathbf{x}},\hat{\mathbf{f}}=\hat{\mathbf{y}}}}{F_{\hat{\mathbf{g}}=\hat{\mathbf{y}},\hat{\mathbf{f}}=\hat{\mathbf{y}}}}}{\tan^2\theta\frac{F_{\hat{\mathbf{g}}=\hat{\mathbf{x}},\hat{\mathbf{f}}=\hat{\mathbf{x}}}}{F_{\hat{\mathbf{g}}=\hat{\mathbf{y}},\hat{\mathbf{f}}=\hat{\mathbf{y}}}}+2\tan\theta\frac{F_{\hat{\mathbf{g}}=\hat{\mathbf{x}},\hat{\mathbf{f}}=\hat{\mathbf{y}}}}{F_{\hat{\mathbf{g}}=\hat{\mathbf{y}},\hat{\mathbf{f}}=\hat{\mathbf{y}}}}+1}. \tag{23}$$

By combining Eq. (23) with Eqs. (14)–(16) the relative flow anisotropy for a hexagonal foam in which gravity is at an angle θ from the vertical can be written as

$$\frac{F_{\hat{\mathbf{g}}=\hat{\mathbf{r}},\hat{\mathbf{f}}=\hat{\mathbf{r}}_\perp}}{F_{\hat{\mathbf{g}}=\hat{\mathbf{r}},\hat{\mathbf{f}}=\hat{\mathbf{r}}}} = \frac{\tan\theta\,\gamma^2+(1-\tan^2\theta)\gamma}{\tan^2\theta(\gamma^2+2)+2\tan\theta\,\gamma+2} \tag{24}$$

At small strains Eq. (24) can be further simplified:

$$\frac{F_{\hat{\mathbf{g}}=\hat{\mathbf{r}},\hat{\mathbf{f}}=\hat{\mathbf{r}}_\perp}}{F_{\hat{\mathbf{g}}=\hat{\mathbf{r}},\hat{\mathbf{f}}=\hat{\mathbf{r}}}} \approx \frac{(1-\tan^2\theta)}{(1+\tan^2\theta)}\frac{\gamma}{2}. \tag{25}$$

This equation implies that, at least at small strains, the highest magnitude for the relative anisotropy occurs at angles of 0° and 90°, which correspond to the two situations that have been examined in the previous sections of this paper. For gravity at 45° to the shear direction there is no flow anisotropy.

IV. OTHER EFFECTS OF SHEAR ON DRAINAGE

A. Length λ of Plateau borders per volume of foam

In addition to flow anisotropy, shear has other impacts on the drainage behavior. The first is the change in the length of the Plateau borders per volume of foam, λ, which affects proportionally both the foam liquid content and the volumetric flow rate through the foam. If A_{av} is the average cross-sectional Plateau border area, then the following relationships holds for average liquid content ε:

$$\varepsilon = \lambda A_{av}. \tag{26}$$

The length of Plateau borders per volume, λ, is a purely geometric quantity and can be obtained from the following equation:

$$\lambda = \frac{\sum|\boldsymbol{l}_i|}{V} = \frac{\sum\sqrt{\Delta x_i^2+\Delta y_i^2+\Delta z_i^2}}{V}. \tag{27}$$

In this work, the Plateau border length per volume is nondimensionalized by dividing by the value for an unsheared foam, λ_0. From Fig. 8 it can be seen that shear increases the total Plateau border length; however, the dependency is weak (in the three-dimensional foam it is a maximum of about a 1% increase) and therefore has only a very minor effect on the drainage.

The two-dimensional equivalent of the length of Plateau borders per volume is the length of edges per area, λ_{2D}. This can be calculated analytically using Eqs. (11), (12), and (27):

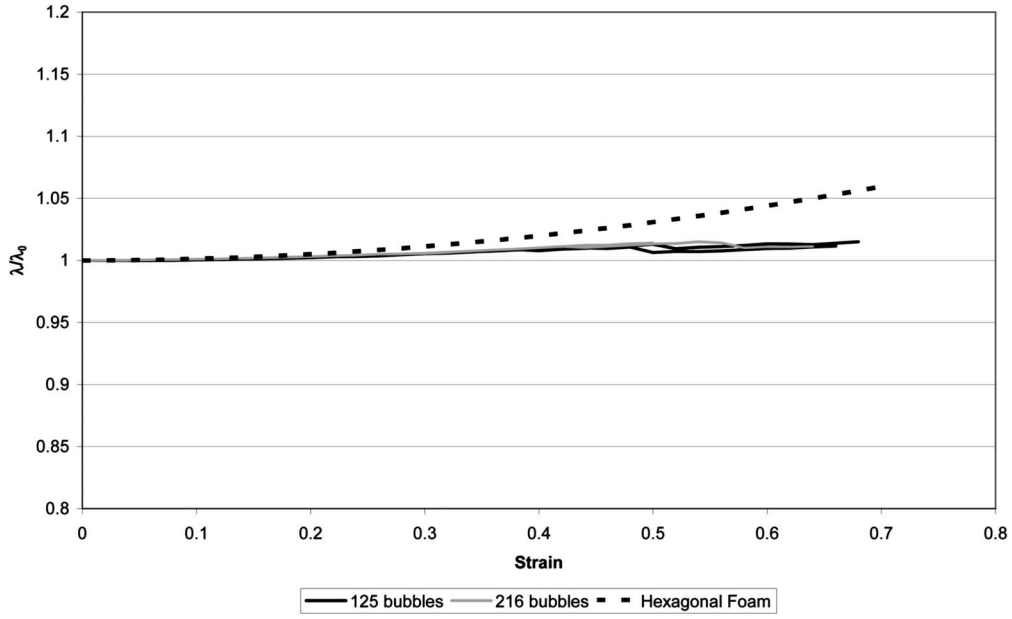

FIG. 8. The effect of shear on the length of the Plateau borders per volume of foam.

$$\frac{\lambda_{2D}}{\lambda_{0,2D}} = \sqrt{\left(\frac{\gamma}{2}\right)^2 + 1}. \tag{28}$$

B. Ratio *m* of the average actual velocity to the macroscopic velocity

If, for instance, gravity is assumed to be in the *y* direction, then the following macroscopic drainage equation holds [7,8]:

$$F_{\hat{\mathbf{g}}=\hat{\mathbf{y}},\hat{\mathbf{f}}=\hat{\mathbf{y}}} = \lambda A_{av}\left(\frac{\rho g}{mC_{PB}\mu}A_{av} - \frac{\sigma\sqrt{\sqrt{3}-\pi/2}}{2mC_{PB}}\frac{1}{\sqrt{A_{av}}}\frac{dA_{av}}{dy}\right). \tag{29}$$

The term in parentheses is the average macroscopic liquid velocity. The factor *m* is the ratio of the average instantaneous liquid velocity to the macroscopic velocity or, stated differently, how much longer the liquid takes to travel through the tortuous Plateau border network than it would through a vertical Plateau border. The parameter *m* is usually assigned a value of 3, which is obtained by assuming that the orientations of the Plateau borders are random [11].

In these drainage calculations there are assumed to be no macroscopic gradients in Plateau border area. This means that the capillary term in Eq. (29) can be ignored:

$$m_{\hat{\mathbf{g}}=\hat{\mathbf{y}}} = \lambda {A_{ave}}^2 \frac{\rho g}{F_{\hat{\mathbf{g}}=\hat{\mathbf{y}},\hat{\mathbf{k}}=\hat{\mathbf{y}}} C_{PB}\mu}. \tag{30}$$

By making the same assumptions as were used to obtain Eqs. (4)–(10), the following equation for *m* can be derived (note that the flow direction of interest is the same as the direction of gravity, $\hat{\mathbf{f}}=\hat{\mathbf{g}}$):

$$m_{\hat{\mathbf{g}}} \approx \frac{\sum |\boldsymbol{l}_i|}{\sum \frac{(\boldsymbol{l}_i \cdot \hat{\mathbf{g}})^2}{|\boldsymbol{l}_i|}}. \tag{31}$$

For instance, for gravity in the *y* direction:

$$m_{\hat{\mathbf{g}}=\hat{\mathbf{y}}} \approx \frac{\sum \sqrt{\Delta x_i^2 + \Delta y_i^2 + \Delta z_i^2}}{\sum \frac{\Delta y_i^2}{\sqrt{\Delta x_i^2 + \Delta y_i^2 + \Delta z_i^2}}}. \tag{32}$$

Figure 9 shows the effect of shear on the value of *m* for flow both parallel and perpendicular to the direction of shear. It can be seen from this figure that shear decreases the average drainage path length in the direction of shear and increases it perpendicular to shear. The reason for this is that shear lengthens Plateau borders that are close to the direction of shear and shrinks those that are close to perpendicular to shear (e.g., Fig. 7). This means that for drainage in the direction of shear, a given element of fluid will have more of its path through the foam consisting of near-vertical fast-flowing Plateau borders than the now shorter more horizontal Plateau borders, and vice versa for drainage perpendicular to the shear.

As with the relative degree of anisotropy, relatively simple relationships can be obtained based on two-dimensional hexagonal foams [from Eqs. (11), (12), and (32)]:

$$\frac{m_{\hat{\mathbf{g}}=\hat{\mathbf{y}}}}{m_0} = \left(\frac{\gamma}{2}\right)^2 + 1, \tag{33}$$

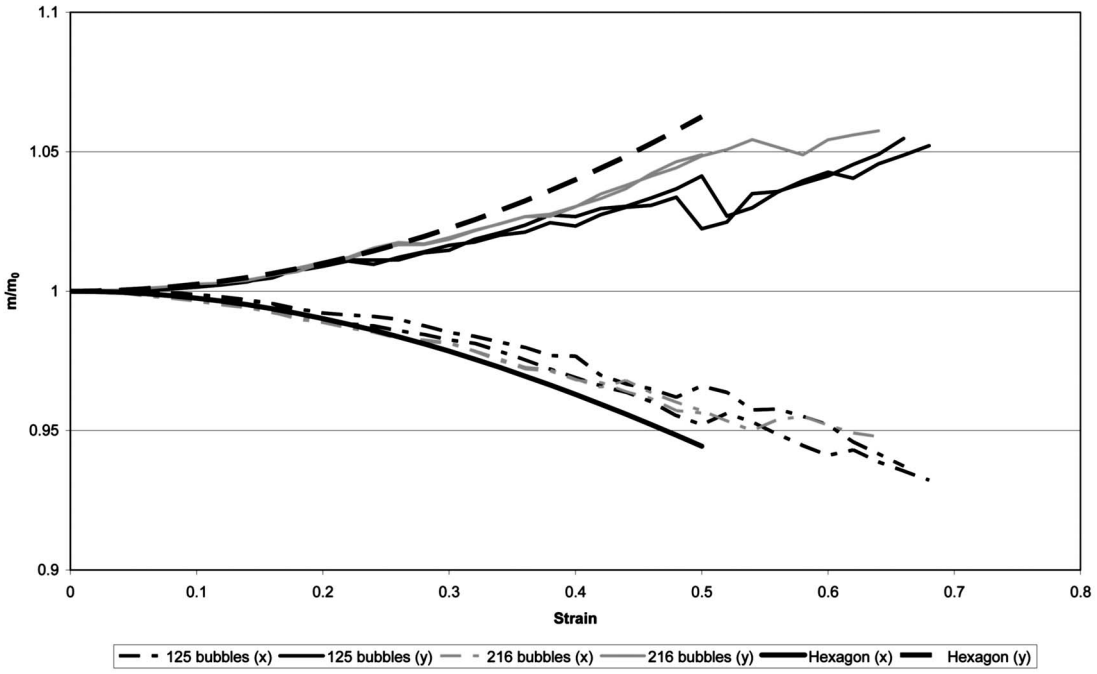

FIG. 9. m/m_0 as a function of strain showing both the three-dimensional simulations and the results from the hexagonal foam. m_0 has a value of 3 for three-dimensional foams and 2 for two-dimensional foams (shear in the x direction).

$$\frac{m_{\hat{\mathbf{g}}=\hat{\mathbf{x}}}}{m_0} = \frac{\left(\frac{\gamma}{2}\right)^2 + 1}{\frac{\gamma^2}{2} + 1}. \tag{34}$$

The agreement between these equations for hexagonal foams and the full three-dimensional simulations can be seen in Fig. 9.

V. THE CONVECTIVE ROLL

A. What is the convective roll in foams?

A standard experiment for investigating the drainage behavior of foams is forced drainage. In these experiments a foam is created in a column and allowed to drain. Once the foam is reasonably dry, a constant flow rate of liquid is added into the top of the foam. The relationship between the speed of the wetting front and the liquid flow rate being added is an important indicator of the drainage processes occurring [7,11]. What has been found, though, is that when the flow rate exceeds a certain critical value, the foam bed no longer remains stationary, but begins to undergo a convective roll [13–15].

What was puzzling is that the onset of the convective roll requires a nonuniform horizontal liquid content in order to generate a strained and ultimately yielding foam. Conventional drainage theory predicts that any horizontal variation in the liquid content should rapidly be smoothed out by capillary suction. One possible explanation that has been proposed is dilatancy [5,6], but while this effect may play a role, no theory based solely on this phenomenon has been able to successfully predict the convective roll.

The reason why the shear-induced flow anisotropy is a possible cause is because it magnifies the effect of slight variations in the horizontal liquid content. A variation in the liquid content causes a local straining of the foam; this straining will result in the flow anisotropy outlined above, which will cause liquid to flow toward the area in which there was already a slight increase in liquid content, causing the fluctuation to grow. If the effect of the flow anisotropy is greater than the restoring ability of capillary suction, then the instability will grow until the foam yields and begins to undergo a convective roll.

B. Predicting the onset of the convective roll

Using the relationships for the anisotropic flux together with existing theory on the response of a foam to an applied strain, a relationship for the liquid content at which the onset of the convective roll will occur can be obtained.

The degree of the relative anisotropy is related to the strain on the foam [from Eq. (18), assuming strain is low, where F_a is the induced flux in the horizontal direction, F_g is the vertical gravity-driven flow, and γ is the applied strain]:

$$F_a \approx \frac{F_g}{2}\gamma. \tag{35}$$

In the forced drainage experiments, the stress on the foam is caused by horizontal variations in the liquid content ε. Horizontal variations in liquid content mean variations in the gravitational force exerted on the foam and thus a shear stress. At equilibrium, the shear stress τ can be written as a function of gradients in the liquid content:

$$\tau = \rho g \frac{d\varepsilon}{dx}. \tag{36}$$

The strain on the foam is related to the shear stress by means of the elastic modulus G:

$$\gamma = \frac{\tau}{G}. \tag{37}$$

Below their yield stress foams act as elastic solids. This is because strain increases the surface area and, therefore, surface energy of the system. The behavior is elastic at small strains, since the foam will return to its original state if there have been no (or very few) topological changes. At higher liquid content the individual bubbles are less deformed for a given strain and so the elastic modulus decreases with increasing liquid content. The elastic modulus is therefore a function of the bubble radius r_b, the liquid content, surface tension σ, as well as the critical liquid content at which the foam loses rigidity, ε_R [11]:

$$G = \frac{k_G \sigma}{r_b}\left(\frac{\varepsilon_R - \varepsilon}{\varepsilon_R}\right)^{\beta}. \tag{38}$$

In this relationship k_G is of the order of unity, while $0.5 < \beta < 0.7$ [11]. k_G is a structural parameter that is related to the rate of film stretching with increasing strain. It does not depend on any of the surfactant or fluid properties, but is likely to be slightly dependent on the polydispersity of the foam. Above a critical strain, large numbers of topological changes occur and the foam deforms irreversibly. The value of this yield strain will influence the liquid content gradient at the point at which the foam yields at the onset of the convective roll, but this simple theory suggests that it does not have a significant influence on whether the convective instability occurs or not.

The other two liquid fluxes to note are the vertical gravity-driven flux F_g (capillary gradients in the vertical direction are ignored) and the horizontal flux caused by capillary suction, F_c. Both these fluxes can be written as a function of the liquid content ε [from Eq. (29), noting that $\varepsilon = \lambda A$], where C_{PB} is the Plateau border drag coefficient, μ is the liquid viscosity, and λ is the length of Plateau borders per volume of foam ($\lambda = k_\lambda r_b^{-2}$, where $k_\lambda \approx 2.6$ for a random monodispersed foam [10]):

$$F_g \approx \frac{\rho g}{3 C_{PB} \mu}\frac{\varepsilon}{\lambda}, \tag{39}$$

$$F_c \approx -\frac{\sqrt{\sqrt{3} - \pi/2}\,\sigma}{6 C_{PB} \mu}\sqrt{\frac{\varepsilon}{\lambda}}\frac{d\varepsilon}{dx}. \tag{40}$$

By combining Eqs. (35)–(39), the horizontal flux due to the flow anisotropy can be written as a function of ε:

$$F_a \approx \frac{(\rho g)^2}{6 C_{PB} \mu}\frac{r_b}{k_G \sigma}\left(\frac{\varepsilon_R}{\varepsilon_R - \varepsilon}\right)^{\beta}\frac{\varepsilon^2}{\lambda}\frac{d\varepsilon}{dx}. \tag{41}$$

For gravity in the same direction as the strain (as is the case here), the anisotropic flux is in the direction of the increase in the foam deflection. This means that the anisotropic flux is in the direction of increasing liquid content. The capillary suction, on the other hand, occurs in the direction down the gradient of liquid content. This means that these two effects oppose one another.

Since the anisotropic flux and the capillary flux are both linearly dependent on the gradient of liquid content, below a critical value of ε, F_c has a larger magnitude than F_a irrespective of the size of the fluctuation in ε. This means that below this critical liquid content, any fluctuations in liquid content will be smoothed out by capillary suction. Above this critical value, though, any fluctuation will grow until the foam yields and the convective roll begins. The critical liquid content ε_C above which instabilities will grow and the convective roll begins is thus the point at which $F_c + F_a = 0$ (note that the relationship is implicit in terms of ε_C):

$$\varepsilon_C = \left[k_g^{\,2} k_\lambda \left(\sqrt{3} - \frac{\pi}{2}\right)\right]^{1/3}\left(\frac{\sigma}{\rho g}\right)^{4/3}\left(\frac{\varepsilon_R - \varepsilon_C}{\varepsilon_R}\right)^{2\beta/3} r_b^{-4/3}. \tag{42}$$

C. Comparison of the predicted onset with experimental values

Assuming that the liquid in the Plateau borders has physical properties similar to those of water and ε_R and β have values of 0.25 and 0.5, respectively, then the relationship between ε_C and r_b can be obtained by solving Eq. (42) numerically (Fig. 10). The critical liquid content does not change as rapidly as the exponent in the power on the bubble radius in Eq. (42) might suggest, since the relationship is tempered by the fact that the elastic strength of the foam decreases as the liquid content increases.

While the shape of the curve in Fig. 10 is qualitatively similar to the relationship obtained experimentally by Weaire *et al.* [15] (Fig. 11), the predicted critical liquid content for a given bubble size is too low. The bubble sizes that correspond to a given critical liquid content are about an order of magnitude too small (the scale in both graphs is the inverse of the bubble size).

Since the critical liquid content is underpredicted, this implies that the relative flow anisotropy is too large, the elastic modulus is too small, or the predicted capillary suction is too small. One possible source of the discrepancy is that the liquid content is assumed to be low in the modeling of the flow anisotropy, while the liquid contents in the experimental data are all quite high. It is already known that the liquid content has an impact on the response of a foam structure to shear [Eq. (38) implies that the interfaces do not deform to the same extent for a given strain as the liquid content increases]. It is therefore reasonable to suppose that the relationship between the relative flow anisotropy and strain will also be a function of liquid content.

A second assumption that may be incorrect and requires investigation is that the foam has the same elastic modulus when the stress is applied by means of internal liquid content variations (as is the case here) as it does when the stress is applied externally [Eq. (38) was obtained for foams with external forces applied to them]. Liquid drainage applies stresses to the walls of the Plateau borders, which will result

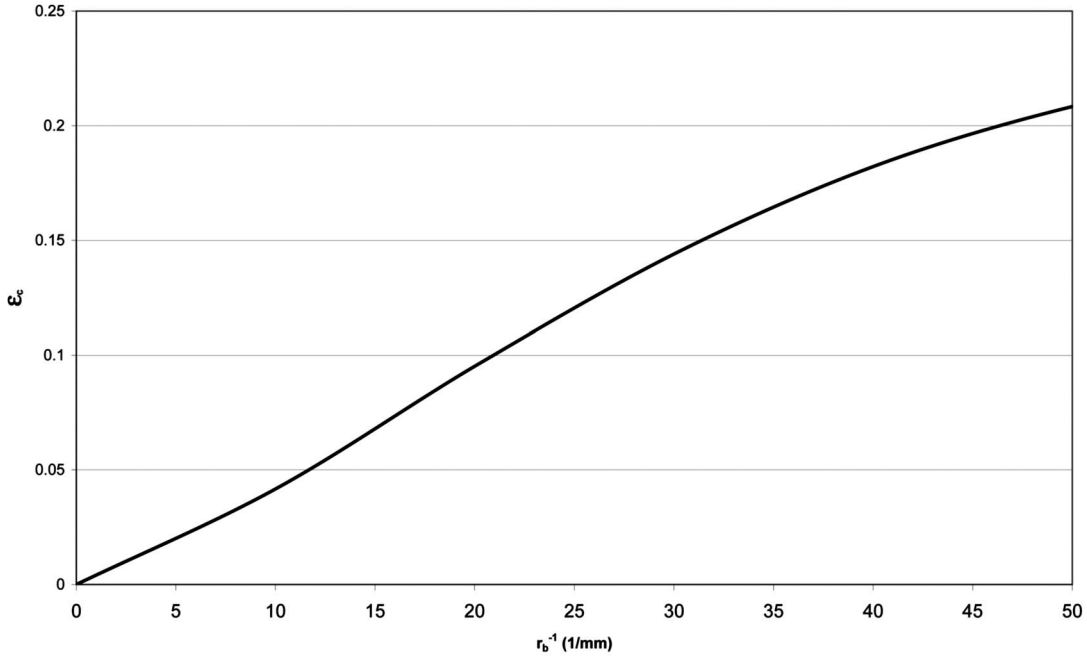

FIG. 10. The critical liquid fraction for the onset of the convective roll as a function of the inverse of the bubble size as predicted from Eq. (42).

in the foam structure deviating from Plateau's rules for the angles at which films meet, since forces other than surface tension will be influencing the structure. That drainage can cause a foam structure to deviate from Plateau's rules has already been observed experimentally [11]. This difference in the way the foam deforms could mean a different relationship for the elastic modulus for internally stressed foams.

VI. CONCLUSIONS AND FUTURE WORK

This paper has shown that shear has a large impact on the drainage behavior of foams. The biggest impact of shear is that it causes the drainage to become anisotropic. This effect is a significant one, with flows being induced in the direction perpendicular to gravity that are up to about 20% of the

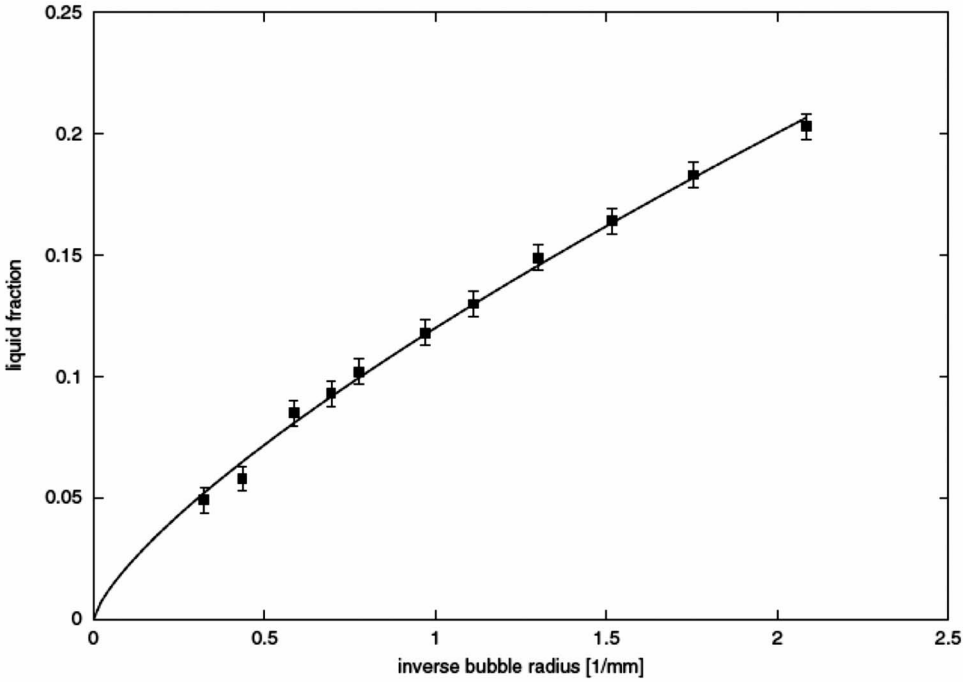

FIG. 11. Experimental relationship between the liquid content at the onset of the convective roll and the inverse of the bubble size (from Weaire *et al.* [15]). Note that the line in this figure is not a theoretical one but is simply a guide for the eye.

primary gravity-driven flow at the point at which the foam yields.

A secondary phenomenon that has been noted is the effect of shear on the resistance of the foam to drainage, with the resistance decreasing with increasing strain for flow parallel to the strain direction, but increasing for flow perpendicular to the strain direction.

The flow anisotropy also provides a possible explanation for the convective roll sometimes seen in forced drainage experiments. A simple theory based on this phenomenon predicts the correct trend for the onset of the convective roll, but it underpredicts the critical liquid content at which it occurs. This means that the simple theory is either overpredicting the flow anisotropy, or underpredicting either the elastic modulus of the foam or the capillary suction.

The two main effects that will need to be investigated in future work will be the influence of liquid content and the polydispersity of the bubbles on the flow anisotropy. These are important since real foam systems are typically polydispersed and the liquid content at which the convective roll usually occurs is high enough that low-liquid-content assumptions become suspect. The main influence that polydispersity is likely to have is that the onset of topological changes will occur at smaller strains and there will be a greater range of strains over which topological changes will occur. This is because the average film size decreases and the range of film sizes increase as polydispersity increases [16]. The yield strain will also decreases with increasing polydispersity. This means that the increase in the flow anisotropy with strain is likely to be lower than that in a monodispersed system and also less linear. The ultimate flow anisotropy as the foam yields is also likely to be lower due to the decrease in the yield strain.

APPENDIX A: EFFECT OF INCLUDING LOCAL LIQUID CONTENT VARIATIONS

It is possible to solve for the drainage within individual Plateau border segments within the foam [using Eq. (1)]. The method involves iteratively improving the volume balance for flows into and out of vertices by locally varying the Plateau border areas until convergence is obtained. The full details of this simulation method are beyond the scope of this paper, but the results of these calculations are all the flows within a foam in which the liquid content is macroscopically uniform, but in which the local variations in liquid content are accounted for. Figure 12 gives a comparison between the results from this-time consuming and complex calculation and the simplified calculation from Eqs. (9) and (10). The full drainage calculation was based on a typical aqueous soap foam ($\mu=0.001$ Pa s, $\rho=1000$ kg/m^3, and $\sigma=0.04$ N/m), with a bubble size of 2 cm and a liquid content of about 0.15%. The close agreement between these results indicates that the assumption of constant Plateau border area does not have a large impact on the results obtained.

APPENDIX B: PROOF THAT REFINING THE STRUCTURE DOES NOT INFLUENCE THE PREDICTED DRAINAGE

This Appendix will show that subdividing the edges has no impact on the results from Eqs. (6)–(8). Assume that an edge has a length l, and components Δx and Δy. Using Eq. (7) on this single edge we have

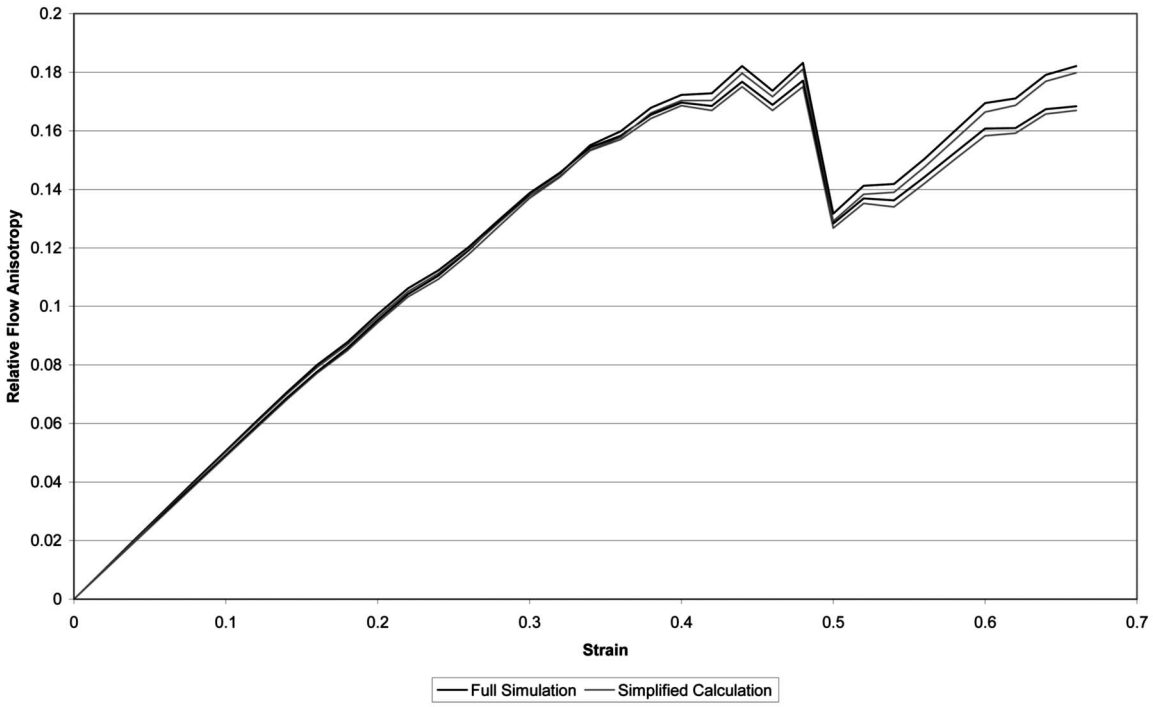

FIG. 12. A comparison between the full drainage simulation and the approximation given by Eqs. (9) and (10) for the relative flow anisotropy (the two lines are $F_{\hat{\mathbf{g}}=\hat{\mathbf{y}},\hat{\mathbf{f}}=\hat{\mathbf{x}}}/F_{\hat{\mathbf{g}}=\hat{\mathbf{y}},\hat{\mathbf{f}}=\hat{\mathbf{y}}}$ and $F_{\hat{\mathbf{g}}=\hat{\mathbf{x}},\hat{\mathbf{f}}=\hat{\mathbf{y}}}/F_{\hat{\mathbf{g}}=\hat{\mathbf{x}},\hat{\mathbf{f}}=\hat{\mathbf{x}}}$).

$$F_{\hat{\mathbf{g}}=\hat{\mathbf{x}},\hat{\mathbf{f}}=\hat{\mathbf{y}}} = K\frac{\Delta x \Delta y}{l} \quad \text{where } K = \frac{\rho g}{VC_{PB}\mu}A^2. \tag{B1}$$

If this edge is subdivided into two pieces labeled 1 and 2 and Eq. (5) is again used to calculate the average flux, we get

$$F_{\hat{\mathbf{g}}=\hat{\mathbf{x}},\hat{\mathbf{f}}=\hat{\mathbf{y}}} = K\left(\frac{\Delta x_1 \Delta y_1}{l_1} + \frac{\Delta x_2 \Delta y_2}{l_2}\right). \tag{B2}$$

Since the edge is simply being subdivided, the slopes of the new pieces will be the same as that of the original edge:

$$\frac{\Delta x_1}{l_1} = \frac{\Delta x_2}{l_2} = \frac{\Delta x}{l}. \tag{B3}$$

This means that, from Eqs. (B2) and (B3),

$$F_{\hat{\mathbf{g}}=\hat{\mathbf{x}},\hat{\mathbf{f}}=\hat{\mathbf{y}}} = K\frac{\Delta x}{l}(\Delta y_1 + \Delta y_2). \tag{B4}$$

$\Delta y_1 + \Delta y_2 = \Delta y$, since each of the new edges is a subsection of the old edge. This means that further subdivision of the edges has no impact on the answer obtained.

[1] F. Rouyer, S. Cohen-Addad, M. Vignes-Adler, and R. Hohler, Phys. Rev. E **67**, 021405 (2003).
[2] H. M. Princen, J. Colloid Interface Sci. **91**, 160 (1983).
[3] H. M. Princen and A. D. Kiss, J. Colloid Interface Sci. **112**, 427 (1986).
[4] D. A. Reinelt and A. M. Kraynik, J. Rheol. **44**, 453 (2000).
[5] D. Weaire and S. Hutzler, Philos. Mag. **83**, 2747 (2003).
[6] F. Rioual, S. Hutzler, and D. Weaire, Colloids Surf., A **263**, 117 (2005).
[7] G. Verbist, D. Weaire, and A. M. Kraynik, J. Phys.: Condens. Matter **8**, 3715 (1996).
[8] R. Leonard and R. Lemlich, AIChE J. **11**, 18 (1965).
[9] K. A. Brakke, Philos. Trans. R. Soc. London, Ser. A **354**, 2143 (1996).
[10] A. M. Kraynik, D. A. Reinelt, and F. van Swol, Phys. Rev. E **67**, 031403 (2003).
[11] D. Weaire and S. Hutzler, *The Physics of Foam* (Clarendon Press, Oxford, 1999).
[12] T. Green, L. Lue, and P. Grassia (private communication).
[13] M. U. Vera, A. Saint-Jalmes, and D. J. Durian, Phys. Rev. Lett. **84**, 3001 (2000).
[14] S. Hutzler, D. Weaire, and R. Crawford, Europhys. Lett. **41**, 461 (1998).
[15] D. Weaire, S. Hutzler, S. Cox, N. Kern, M. D. Alonso, and W. Drenckhan, J. Phys.: Condens. Matter **15**, S65 (2003).
[16] A. M. Kraynik, D. A. Reinelt, and F. van Swol, Phys. Rev. Lett. **93**, 208301 (2004).